CRN-PN/ 89-27

PARITY DEPENDANCE IN THE OPTICAL POTENTIAL OF SD-SHELL NUCLEI

J.L. FERRERO and J.A. RUIZ
Instituto de Física Corpuscular, Universidad de Valencia-CSIC, Burjasot, Valencia, Spain

B. BILWES, R. BILWES
Centre de Recherches Nucléaires et Université Louis Pasteur, Strasbourg, France

CENTRE DE RECHERCHES NUCLEAIRES

STRASBOURG

IN2P3 CNRS

UNIVERSITE LOUIS PASTEUR

si f

To be published in Nuclear Physics

PARITY DEPENDENCE IN THE OPTICAL POTENTIAL OF SD-SHELL NUCLEI *

J. L. FERRERO and J. A. RUIZ

Instituto de Física Corpuscular, Universidad de Valencia-CSIC, Burjasot, Valencia, Spain.

B. BILWES and R. BILWES

Centre de Recherches Nucléaires and Université Louis Pasteur, Strasbourg, France.

Abstract: Elastic scattering between sd-shell nuclei differing by one,two, three and four nucleons has been measured. The oscillating pattern of the angular distributions, when it is observed, is attributed to the interference between direct elastic scattering and elastic transfer. Explicit DWBA treatment of the elastic transfer or parity dependent real potential analysis allow both a good reproduction of the data. The sign and the importance of the parity potential deduced by fitting the data are in good agreement with the predictions of microscopic calculations in the two centre shell-model.

NUCLEAR REACTIONS ^{32}S(^{31}P,^{31}P), E_{lab} = 86.5 MeV; ^{28,29}Si(^{31}P, ^{31}P), E_{lab} = 85.9 MeV; ^{27}Al(^{31}P,^{31}P), E_{lab} = 79.5 MeV; ^{30}Si(^{32}S,^{32}S), E_{lab} = 90 MeV; ^{36}S(^{32}S,^{32}S), E_{lab} = 90,97 MeV; ^{40}Ca(^{37}Cl,^{37}Cl), E_{lab} = 120.5 MeV; measured σ(E,θ); elastic transfer EFR-DWBA analysis; deduced spectroscopic factors; parity dependent folding model analysis.

---

* Work partially supported by CAYCIT (Spain) under project PB 0415 1988/90 and by IN2P3-CNRS (France)

1. Introduction

The optical model is the most widely used model to analyse heavy-ion elastic scattering. The standard optical model potential is taken as a local potential with negative real and imaginary parts which rise quickly and monotonically to zero in the surface region as in the Woods-Saxon or in the folding form-factors. Nevertheless in many (asymmetric) systems it seems necessary to include a parity-dependent term in order to reproduce the experimental data [1-10]. Usually it is taken real but a complex one has been used in some systems [3,4]. In both cases this term produces oscillations in the angular distribution. These oscillations are at intermediate angles when the energy is near the Coulomb barrier and move to backward angles when the energy increases [1]. Similar oscillations can be produced also by allowing a certain degree of surface transparency in the standard optical potential, but in that case their phase changes rapidly with the energy contrary to the oscillations produced by the parity dependence. In some systems as $^{28}Si+^{32}S$, $^{16}O+^{18}O$ and others(see refs. 1,7,8), this characteristic permitted to rule out the surface transparency in favour of the parity dependence. In other cases (e.g. $^{16}O+^{20}Ne$, $^{28}Si+^{16}O$, ^{12}C) it seems that both mechanisms are present [2,3]. In particular the surface transparency enhances the cross section at large angles (ALAS) and permits the shape resonances (gross structures) to appear in the excitation function. The parity dependence is responsible for a further enhancement and, specially, for doubling the periodicity of such resonances [11]. This latest effect was seen also in inelastic and transfer excitation curves [12] and even in the fusion excitation curve of the $^{12}C+^{16}O$ system [15].

One possible reason for a parity dependence in the optical potential is that it simulates the presence of the elastic transfer reaction which consists in a transfer between target and projectile of the nucleons which differenciate both nuclei in such a way that the output channel is identical to the elastic one. As a consequence of this indistinguibility both processes interfere and produce the oscillations mentioned above which phase is slowly energy dependent. Probably this is the obvious explanation for the parity dependence detected in systems of similar mass nuclei and, indeed, a parity dependence should be included into the optical analysis of the many systems which evidence such an elastic transfer [1,9,13,14]. It is not clear if that explanation is suitable for the case of very asymmetric systems as $^{16}O+^{28}Si$ or $^{12}C+^{28}Si$. The difficulty to predict the cross section in such many nucleons transfers does not allow a reliable conclusion. Moreover the data can be, in principle, reproduced by using a model independent optical potential which can display oscillating features but in every case is not l-dependent. This has been done at least in the case of $^{16}O+^{28}Si$ scattering [16] and casts some doubts about the necessity of a parity dependence in such systems.

On the other hand, on a microscopic point of view, it can be argued that elastic scattering and elastic transfer are indistinguishable because of the indiscernibility of the nucleons in both colliding nuclei. Thus the parity dependence turns to be an effect of the necessary antisymmetrization between all the nucleons of the system. Taking into account the elastic transfer is equivalent to use only a partial antisymmetrization and we can expect that a fully microscopic calculation would give different results, specially for very asymmetric systems. The theories taking into account the full antisymmetrization (RGM or GCM) are difficult to apply to heavy ions owing to the large number of nucleons involved. Qualitative studies in the framework of the RGM show that the antisymmetrization effects introduce a parity dependence in the heavy-ion optical potential as it was evident from the exact calculation in the case of two light-ions scattering [23]). Moreover, recently D.Baye proposed a model [24]) based on the GCM which permits to investigate qualitative characteristics of the parity dependence and applied it to a considerable number of systems in the sd-shell. It is interesting to test the validity of these calculations in order to give support to his predictions for systems where the origin (or even the presence) of a parity dependence is controverted and to encourage possible extensions of the model (already proposed in ref. [24])) and further theoretical and experimental work.

For this reason we have measured the elastic scattering in seven systems studied by Baye and analysed the data in order to test the model predictions. In section 2 we describe the experimental method briefly. In section 3 we evaluate the contribution of the elastic transfer to the experimental data, in these systems and in two others we had measured previously, by DWBA calculations. In section 4 the systems which evidence the presence of elastic transfer are analysed by means of a parity dependent term and the characteristics of this term are studied. We compare the results of section 4 with the model predictions in section 5 and we summarize and give the conclusions in section 6.

2. Experimental method

The experiments have been performed at the MP accelerator of the CRN-Strasbourg. Angular distributions of elastic scattering of ^{31}P ,^{32}S and ^{37}Cl on different targets were measured between 30 and 130 degrees in the c.m. system. The incident energies were chosen so that the rainbow angle would be almost the same for all mass systems. As we are mainly interested in the possible interferences between potential elastic scattering and elastic transfer amplitudes (see eq. 1 below) this angle was chosen close to 60° c.m.. This means that the transfer peak is expected at $\sim$ 120° c.m. and consequently the eventually oscillatory pattern will be observable in good conditions at intermediate angles.

The elastic scattering of ^{31}P + ^{32}S was measured at 86.5 MeV-lab, ^{31}P + $^{28,29}Si$ at 85.9 MeV-lab, ^{31}P + ^{27}Al at 79.5 MeV-lab , ^{32}S + ^{30}Si at 90 MeV-lab, ^{32}S + ^{36}S at 90 and 97 MeV-lab and ^{37}Cl + ^{40}Ca at 120.5 MeV-lab. Moreover two angular distributions previously measured are included into the analysis: ^{32}S + ^{34}S at 97.1 MeV-lab and ^{32}S + ^{28}Si at 90 MeV-lab [10]).

The targets were obtained either by the implantation technique [17]) in the case of ^{32}S and ^{36}S (2-3$\mu g/cm^2$) in carbon foils (26$\mu g/cm^2$) [18]) , either by evaporation [19]) of enriched ^{40}Ca, ^{27}Al, or SiO_2 (about 20 $\mu g/cm^2$ in every case) on carbon foils (20 $\mu g/cm^2$).

The data have been taken using the kinematical identification method with two position-sensitive solid-state detectors mounted in coincidence, which has been described previously [20,21]). On-line analysis was performed in order to get a permanent check of the detectors' behaviour and to optimize the experimental conditions (target orientation, statistics..) [22]).

The choice of the distance between the detectors and the targets was determined by the necessary mass and energy resolutions in each case. In this method these quantities are directly related to the angular precision. The distance was 120 mm in the ^{32}S + ^{36}S case, 160 mm in the ^{32}S + ^{30}Si and ^{37}Cl + ^{40}Ca cases, 180 mm in the ^{31}P + $^{28,29}Si$, ^{27}Al cases and 240 mm in the ^{31}P + ^{32}S case. A typical energy resolution of 500 keV was obtained which allowed to separate elastic events from inelastic ones. As the angular resolution was in every case better than 0.5 degrees in the lab the events were stored in steps of 1 degree in the c.m..

For each angular distribution a few different geometrical settings of the detectors were sufficient to obtain the whole angular distributions. The error bars include both the statistical and the relative normalization errors between the different measurements. Absolute values of the elastic cross sections were obtained by normalizing to the Rutherford scattering at the most forward angles.

3. Elastic transfer analysis

In the first analysis of the data we have taken into account explicitely the elastic transfer by adding to the direct elastic scattering amplitude, obtained from a standard optical potential, the transfer amplitude calculated by the DWBA. The transferred nucleons were represented by the extreme-cluster model. Thus the "observable" scattering amplitude

$\tilde{f}$ is given by

$$\tilde{f}_{M_a M_A, M'_a M'_A}(\theta,\phi) = \delta_{M_a M'_a}\delta_{M_A M'_A} f^{(el)}(\theta,\phi) + (-1)^{2I} f^{(tr)}_{M_a M_A, M'_A M'_a}(\pi-\theta,\phi+\pi) \quad (1)$$

where I is the spin of the smaller nucleus, either A or a. The δ symbols in this formula reflect the fact that the spin orientation does not change in the elastic scattering because the standard optical potential is spin-independent (till now there is no clear evidence for a sizeable spin dependence in heavy-ion interactions [25])). On the contrary it is, in principle, possible that the spin orientation after the transfer reaction may be different from the initial one. On the other hand the cross section is obtained from $\mid \tilde{f} \mid^2$ by summing over the final spin orientations (M'_a, M'_A) and averaging over the initial spin orientations (M_a, M_A). Thus in that sum there are two amplitudes ($f^{(el)}$ and $f^{(tr)}$) when $M'_a = M_a$ and $M'_A = M_A$, which interfere producing oscillations in the angular distributions while only the transfer amplitude remains in the other cases contributing incoherently to the cross section. This means that in general only a part of the elastic transfer contributes coherently to the measured cross section while the rest tends to wash out the characteristic interference pattern. Taking into account that the transfer amplitude is calculated in the DWBA without spin dependent potentials it is easy to show that at a given angle θ the transfer cross section which adds coherently is

$$\frac{2j_1+1}{(2I_a+1)(2I_A+1)}\sigma_{l=0}(\pi-\theta)$$

being $\sigma_{l=0}$ the part of the transfer cross section corresponding to a transferred angular momentum $l=0$ and being j_1 the total spin of the transferred particle.

For the optical potential generating $f^{(el)}$ we took the form

$$V_{opt}(r) = NV_F(r) + iW(r) + V_C(r) \quad (2)$$

where $V_C(r)$ is the Coulomb potential for a uniform charge distribution of radius $R = 1.2(A_1^{1/3} + A_2^{1/3})$ fm, $W(r)$ is the Woods-Saxon form factor with well-depth W, radius R_W and diffuseness a_W, and $V_F(r)$ is the folding potential [31]) which is multiplied by a renormalization factor N. In the calculation of $V_F(r)$ we have used the M3Y nucleon-nucleon interaction [26]) and the nuclear densities deduced from charge densities assuming that the neutron and proton distributions are the same and taking into account the finite size of the charge distribution of the nucleons. The charge densities used were deduced from electron scattering as reported in ref [27]), except for the case of ^{34}S where we used the nuclear density obtained from 1 GeV proton scattering [28]).

We determined the free parameters of V_{opt} by fitting the data [29]) but without forcing to fit also the data at backward angles ($\theta_{cm} > 110°$) when there are oscillations as we

were trying to see if such oscillations arise from the elastic transfer. Moreover we fixed the well-depth of the imaginary potential to $W = 50$ MeV in order to reduce the number of parameters. This particular choice of W was verified to be without importance. The same quality of fits were obtained by changing W unless we chose a small value of W (< 5 MeV). This is due to the strong volume absorption produced by such a deep imaginary potential which makes the scattering sensitive only to the tail of the optical potential and consequently relates W and R_W by the Igo ambiguity. It is worth mentioning that fixing the value of W does not prevent a surface transparency of the optical potential which is certainly present in some heavy ion systems.

The values of the V_{opt} parameters obtained from the data are reported in table 1 with a few characteristic quantities as the grazing angular momentum l_g, the reaction cross section σ_R, the strong absorption radius R_{SA} and the values of the real and imaginary potentials at R_{SA}. The fits can be seen in figures 1 to 5 (dashed lines). We observe that the theoretical angular distributions produced by V_{opt} have the typical profile of the heavy-ion scattering at energies near the Coulomb barrier when it is dominated by strong absorption and that they fit very well the experimental data except for the presence of oscillations in some systems. We have verified that it is not possible to reproduce such oscillations with an optical potential of the form (2). The only way to produce oscillations at backward angles without destroying the fit in the rainbow region was to use a small imaginary well-depth ($W < 5$ MeV), which is considered unrealistic for heavy-ion scattering [30]), and even in this case the data reproduction was not very good. This indicates that the origin of these oscillations must be the elastic transfer. We will come back to this point later.

In table 1 the mean value of the renormalization factor is $< N >= 1.34 \pm 0.17$ which is a little bit high in comparison with the value $< N >= 1.06 \pm 0.11$ obtained in a similar analysis by Satchler and Love [31]) of 67 heavy-ion systems. This may be justified because the neutron distribution is not equal to the proton distribution as we supposed for simplicity, specially when the number of neutrons and protons are very different (v.g. in the ^{36}S case). Moreover the incident energies of the present data are near the Coulomb barrier and lower than the energies for the data in ref. [31]). This can be a reason for the value of $< N >$ to be greater than 1 as it reflects the threshold anomaly [32]).

The characteristics of the bound states, the values of the binding potential parameters and the spectroscopic factors given in table 2 are those used in the DWBA transfer calculations [33]) . The resulting curves are presented in figures 1 to 5. The dash-dotted curve is the transfer cross section and the full curve is the total elastic cross section obtained from (1). We can see that the reproduction of the data is in general very good except perhaps at the more backward angles in some systems. An interesting feature of the elastic transfer is

σ/σ_R

$^{31}P + ^{32}S$

$E = 86.5$ MeV

that, the entrance and exit channels being equal, only one spectroscopic factor and one optical potential are involved in the DWBA calculation. This eliminates the indetermination arising from the exit channel optical potential which is normally unknown in the common DWBA calculations. Moreover the spectroscopic factor can be determined directly from the data and not only as a product of spectroscopic factors as in the common case.

For the systems which data show a well-developed oscillatory pattern the spectroscopic factors obtained in this work are in general agreement with others when they are available, either deduced from light-ion scattering or calculated theoretically (see table 2). This fact supports the elastic transfer to be at the origin of the backward angle oscillations observed in these data.

This is obvious in the case of one proton transfer (^{32}S+^{31}P) because the same spectroscopic factor as with light-ion scattering was obtained, as it is generally found for the well-matched one nucleon transfers [1,14]. It is justified in the ^{32}S+^{28}Si and ^{32}S+^{30}Si cases in view of the spectroscopic factors obtained although there are discrepancies with the data at the more backward angles for the latter system. For the other two nucleons transfer cases (fig. 2) the quality of the fits and the reasonable values of the deduced spectroscopic factors support also this conclusion. In the case of ^{31}P+^{28}Si the spectroscopic factor deduced in this work is greater than the one obtained in the ^{28}Si(α,p)reaction [36]. We think that this discrepancy does not weak our conclusion but could indicate that the mechanism of the three nucleons transfer is different in the two reactions. Nevertheless a stronger test of the origin of such oscillations would be to follow their behaviour with the energy. We did not perform measurements at various energies for the systems measured specially for this work (see section 2) but we previously studied in detail the evolution of ^{32}S+^{28}Si elastic scattering with the incident energy. In ref. [7]) we reported 25 angular distributions at energies ranging from 90 to 102 MeV. We concluded from the stability of the oscillations with the energy that their origin is the elastic transfer. For the system ^{32}S+^{34}S the data at three incident energies are available and the same kind of analysis leads to the same conclusion.

For the systems where no clear oscillations are observed only an upper limit of the spectroscopic factors can be given.

The low statistics at backward angles of the data for the ^{37}Cl+^{40}Ca system prevent obtaining significant information about the corresponding elastic transfer. However DWBA calculations with a relatively high value of the spectroscopic factor ($\tilde{S} = 1$) predict (see fig. 3) a very small yield for such a transfer as it is expected intuitively. Therefore it will not produce measurable effects on the total cross section.

σ/σ_R

1

0.1

For the case of $^{31}P+^{27}Al$ the transferred momentum can take values ranging from $l = 0$ to $l = 4$, the $l = 0$ component beeing negligeable in comparison with the $l = 2, 4$ ones (see fig. 5). As it was mentioned before only the $l = 0$ component interferes with the direct elastic scattering. Thus the predicted oscillations in this system have very small amplitudes. It would be necessary to measure with a great precision to observe such kind of oscillations and possibly extract a spectroscopic factor. From our data we could only deduce an upper limit ($\tilde{S} \leq 0.24$) which is comparable to the value of the spectroscopic factor obtained in the $^{32}S+^{28}Si$ case. This is compatible with the equality of the theoretical values in both cases [47]). (The absolute values from experiments depend rather strongly on the binding potential and the optical potential used and consequently the direct comparison with the theoretical values is difficult. The comparison of relative values is more significant).

The angular distribution at 90 MeV for the $^{32}S+^{36}S$ system does not show evident oscillations but is compatible with values of the spectroscopic factor up to $\tilde{S} = 0.24$ that is rather high for a 4n transfer. The data at 97 MeV have too low statistics at backward angles to be usefull in this respect.

In conclusion, at least in the intermediate angle region ($\theta_{cm} \leq 130°$) it is clear that the oscillations observed in some of the studied mass systems are produced essentially by the elastic transfer and conversely when the transfer cross sections are expected to be very low no oscillations are observed.

4. Analysis with a parity dependent optical potential

Let us suppose that the projectile a is composed by the ejectile b plus x nucleons. Schematically a transfer reaction can be written

$$(b + x) + A \longrightarrow b + (A + x)$$

If the b and A nuclei are identical the residual nucleus B formed by the target A plus x nucleons is the same nucleus as the projectile. Thus we have two indistinguishable reactions, $A(a, a)A$ which is the direct elastic scattering and $A(a, b)B$ which is the elastic transfer. As both reactions are physically indistinguishable we must add the corresponding scattering amplitudes to obtain the observable amplitude. This is the point of view of the precedent section. On the other hand we can describe the system by a wave function properly symmetrized with respect to the two (identical) nuclei A and b. If, for simplicity, we suppose the nuclei a and A whithout spin the wave function Ψ reads

$$\Psi = u(\mathbf{r}_\alpha) \mid aA > + u(-\mathbf{r}_\beta) \mid bB > \qquad (3)$$

σ/σ_R

1

where the function $u(\mathbf{r}_\alpha)$ describes the relative motion of the colliding particles a and A and the ket $\mid aA >$ their intrinsic states. The vector $\mathbf{r}_\alpha$ or $\mathbf{r}_\beta$ relies the center of mass of A and a or B and b respectively (see figure 6). Projecting the equation $(H - E)\Psi = 0$ over $< aA \mid$ we obtain an equation which determines $u(\mathbf{r})$

$$\{T_{\mathbf{r}_\alpha} + V_{opt}(r_\alpha) + (\varepsilon - E)\}u(\mathbf{r}_\alpha) + \int \mathrm{d}\mathbf{r}_\beta K(\mathbf{r}_\alpha, \mathbf{r}_\beta)u(-\mathbf{r}_\beta) = 0 \qquad (4)$$

where $T_{\mathbf{r}_\alpha}$ is the kinetic energy operator, V_{opt} is the optical potential between a and A, ε is the intrinsic energy of these nuclei and K is the kernel which appears in the CRC equations (e.g. see ref. [38])). It is clear that including the elastic transfer reaction directly in the wave function (3) leads to add a non-local term to the optical potential. Equation (4) can be solved by an iterative method. The first iteration gives the amplitude expressed in equation (1) of the precedent section. The small range of non-locality of K suggests another possible approximation, that is to substitute the non-local potential by some kind of local equivalent potential transforming (4) into

$$\{T_{\mathbf{r}_\alpha} + V_{opt}(r_\alpha) + (\varepsilon - E) + V_p(r_\alpha)P\}u(\mathbf{r}_\alpha) = 0 \qquad (5)$$

where P is the parity operator $Pu(\mathbf{r}) = u(-\mathbf{r})$. It is easy to solve this equation with the usual optical model codes because when expressed in terms of partial waves the parity dependent term $V_p(r)P$ reads simply $V_p(r)(-1)^l$. What is remarkable is that, if $V_p(r)$ is correctly chosen, equation (5) (which implies much less calculations than formula (1) of precedent section) will take into account the elastic transfer not only in the first order but in all orders.

In the deduction of equations (4) or (5) we supposed that the colliding nuclei do not have a spin. In the general case when one or both nuclei have a spin these equations are not applicable unless the spin orientation cannot change in the transfer reaction. For the systems where the spin can change in the transfer most part of the transfer cross section becomes incoherent with the elastic cross section making unnecessary a parity dependent term in the optical potential. For this reason we did not analyse the ^{37}Cl+^{40}Ca and ^{31}P+^{27}Al systems with a parity dependent potential. Moreover the angular distributions do not show an oscillating structure in such systems.

For the other mass systems studied in this work we applied equation (5) with the optical potential V_{opt} given in table 1 and the parity dependent potential of the form

$$V_p(r) = (-1)^{2I_A} N_p \int \mathrm{d}\mathbf{r}_{bx}\phi(r_{bx})V_{Ax}(r_{Ax})\phi(r_{Ax}) \qquad (6)$$

σ/σ_R

$^{31}P+^{32}S$

which is obtained eliminating the term $V_{Ab} - V_{opt}$ in the kernel $K(\mathbf{r}_\alpha, \mathbf{r}_\beta)$, neglecting the non orthogonality term and the recoil [38]). The parameter N_p can be fitted in order to correct these approximations. It takes into account also the spectroscopic factor. The transferred particle is denoted by x while $\phi(r_{bx})$ and $\phi(r_{Ax})$ are the bound wave functions corresponding to x in the projectile ($a = b + x$) and in the residual nucleus ($B = A + x$) respectively (see figure 6), V_{Ax} being the binding potential which generates this bound state. We used for V_{Ax} the binding potentials of table 2. Finally the sign $(-1)^{2I_A}$ in equation (6), where I_A is the spin of the core nucleus ($I_A = I_b$) arises because in the systems where I_A is not an integer the plus sign in (3) must be changed by a minus sign (i.e Ψ is antisymmetrized in respect to A and b).

By fitting the N_p parameter it was possible to obtain theoretical angular distributions (see figures 7 to 10) practically identical to the full curves in figures 1 to 5 which were obtained with an explicit treatment of the elastic transfer by means of the DWBA approximation (sect. 3). This means that the parity dependent potential given in (6) is adequate to generate a local potential equivalent to the non-local potential in equation (4), the approximations implicit in (6) being corrected by N_p. Moreover it means that the transfer proceeds in one step as it is supposed by the DWBA. This conclusion is generally found in similar analyses of elastic transfer from other systems [1]) when a deep imaginary potential is used.

We have investigated what are the characteristics of $V_p(r)$ which are determined by the experimental data. Other forms for $V_p(r)$ different from (6) were tested. In particular we made $V_p(r)$ proportional to the folding potential $V_p(r) = CNV_F(r)$ and we took also a Yukawa form factor $V_p(r) = N_\beta e^{-\beta r}/r$ with different values for β. By fitting the parameters C and N_β we could obtain in many cases theoretical curves very similar to the ones represented in figures 7 to 10. The corresponding potentials are equivalent to the potential of (6). In figure 11 we have represented a few of such equivalent potentials for the system ^{32}S+^{28}Si. We see that they all have the same value at a radius which is very close to the strong absorption radius R_{SA}. It is clear also that the scattering is insensible to the inner part of the potentials. We have verified this point by "cutting" the potential $V_p(r)$ of equation (6) at a radius R_c into the form

$$V_p(r) = \begin{cases} V_p(R_c) & \text{if } r < R_c \\ V_p(r) & \text{if } r \geq R_c \end{cases}$$

and observing the theoretical curve. For all the systems the theoretical prediction was unchanged for R_c less than ≈ 9 fm. This restricts the sensitivity region of $V_p(r)$ to a zone of about 2 fm around the strong absorption radius which in these systems is approximately 10 fm (see table 1). In consequence we have characterized the importance of $V_p(r)$ for each

particular system by the ratio $V_{pp} = \mid V_p(R_{SA})/NV_F(R_{SA}) \mid$. Moreover in the sensitivity region the sign of V_p is determined without ambiguity because a change of the sign must produce a 180° shift in the theoretical oscillations (as it is evident from the deduction of equation (5)).

5. Comparison with Baye's model

In ref. [24]) Baye derived the properties of the parity dependent part $V_p(r)$ of the optical potential from expectation values of the microscopic hamiltonian calculated with parity-projected wave functions constructed in the two-centre harmonic oscillator shell-model. Representing the range of $V_p(r)$ by the parity radius R_p beyond which the parity dependence becomes negligible the model of ref.[24]) indicates that R_p essentially depends on the difference $\delta = A_1 - A_2$ between the mass numbers A_1 and A_2 of the colliding nuclei, but it is influenced also by the shell structure of the colliding nuclei. For the parity effects to be observable in the experimental data R_p must be greater than, or close to, the strong absorption radius R_{SA}. Nevertheless the value of R_p cannot be determined unambiguously from the data because it depends on the particular form taken for the parity dependent potential $V_p(r)$. As it was shown in section 4 the ratio V_{pp} between $V_p(r)$ and the real part of the standard optical potential at R_{SA} is more suitable to represent the importance of $V_p(r)$ because it is stable upon a change in the $V_p(r)$ form.

In table 3 we compare both quantities V_{pp} and R_p. The parity radius R_p is greater than R_{SA} for the system $^{31}P+^{32}S$ which, as deduced from the experimental data in section 4, shows the most important parity dependence ($V_{pp} = 0.16$). Disregarding the case of $^{32}S+^{36}S$ the other systems show also a parity dependence although they have a parity radius R_p which is up to three fermis below R_{SA}. This is not against the validity of the model because the harmonic oscillator shell-model does not provide wave functions with a good asymptotic behaviour and we expect that R_p will increase up to $R_p \geq R_{SA}$ for such systems if it is obtained with more realistic wave functions. On the contrary, the small value of R_p for $^{32}S+^{36}S$ indicates that the tail of the wave functions is unimportant for the evaluation of R_p in such a system and its value would remain essentially the same in a more realistic calculation. From the analysis of our data we deduced an upper limit of 0.01 for V_{pp}. With this value (i. e. $V_p(r)$ is only 1% of the optical potential real part) the parity dependence produces small oscillations which we cannot rule out from the data (see fig. 10). We can expect that a precise measure of the differential cross section for $\theta > 100°$ would lower the possible value of V_{pp} making negligible the parity dependence in agreement with Baye's prediction.

-V
(MeV)

32 28

Although both V_{pp} and R_p show that the parity effect increases when the nucleon number difference $\delta = A_1 - A_2$ decreases, the parity radius for systems with a fixed δ-value may vary because of differences in the internal structure of the colliding nuclei. This is the case of the three systems with $\delta = 2$ of table 3 . The parity radius R_p is almost the same for ^{31}P+^{29}Si and ^{32}S+^{30}Si but diminishes for ^{32}S+^{34}S due to the change of the subshell [24]). This is partially supported by the behaviour of V_{pp} which diminishes from ^{32}S+^{30}Si to ^{32}S+^{34}S but is unexpectedly small for the system ^{31}P+^{29}Si. This may indicate that not only the number of nucleons which differenciates both colliding nuclei and the subshell involved are important but also what kind of cluster can be formed with such nucleons (d,2n,2p,etc..). Concerning this point it would be interesting to compare experimentally the ^{32}S+^{36}S and ^{32}S+^{36}Ar systems. Both have a similar predicted parity radius (R_p = 3.2 and 2.8 fm respectively, see ref.[24])). Thus according to the model a parity dependent term is not necessary to fit the experimental data but, from the point of view of section 3, while the elastic transfer in the system ^{32}S+^{36}S must be negligible because there are four neutrons involved, it could be important in the case of ^{32}S+^{36}Ar because the four transferred nucleons can form an alpha particle.

The sign of $V_p(r)$ near the parity radius can be also calculated from the model of ref.[24]) and it is unambiguously determined by the experimental data as it was pointed out in the precedent section. In table 3 we compare the sign deduced from the model and from the experiment observing that they agree for all the analysed systems. The sign predicted by the model is also in agreement with analyses of experimental data for other systems with $\delta \leq 4$ as ^{18}O+^{16}O,^{29}Si+^{28}Si ,^{30}Si+^{28}Si and ^{20}Ne+^{16}O [1,2]). We can conclude that Baye's model successfully predicts the sign of $V_p(r)$ for systems with a nucleon number difference $\delta \leq 4$ and describes reasonably well the importance of such a parity potential although the internal wave functions representing the colliding nuclei may be oversimplified.

Concerning more asymmetric systems ($\delta \geq 4$) the model has been applied to a few cases in ref.[24]) and it does not predict a sizeable parity effect. This is verified by the experiment for the ^{32}S+^{24}Mg and ^{32}S+^{40}Ca systems where analyses with a standard optical potential (eq. 2) could reproduce the data [39,40]). On the other hand the oscillating structure which appears in the differential cross section at backward angles for the ^{24}Mg+^{16}O system has been attributed [41]) to the elastic transfer process which proceeds principally through the (sequential) 2α transfer mechanism. This hypothesis is supported by the α-cluster structure of 4N nuclei as ^{24}Mg. The fact that neither this α-cluster structure nor the sequential transfer mechanism are included in the model of ref. [24]) may induce a underestimate of the parity effects for systems as the above mentioned.

Finally we comment briefly the case of ^{16}O+^{28}Si scattering. It is quite clear from

the analysis of the ^{12}C cluster elastic transfer in ref. [42]) that this is not the mechanism responsible for the parity dependence apparently present in this system because it was necessary to add a phase shift to the DWBA amplitude in order to reproduce the data. This phase shift may simulate a 3α sequential transfer which could be a more favoured process than a single ^{12}C transfer. The sequential process generates a parity potential with an imaginary component [43]) contrary to the single step process (see section 4). This would justify the kind of parity dependent term used in ref. [3,4]). Nevertheless this system shows a great surface transparency which can reveal characteristics of the optical potential usually hidden in systems dominated by strong absorption. For instance the deduced optical potential can have oscillating features [16]) which in turn may arise from a strong coupling with inelastic or transfer channels [44,45]).

6. Conclusions

Systematic study of the elastic scattering of nuclei belonging to the sd-shell and differing by one to four nucleons was pursued. The angular distributions were measured on a large angular range at energies near the Coulomb barrier. A general good reproduction of the data was obtained by optical model analyses with folding potentials calculated with the M3Y interaction. Nevertheless a renormalization of the potentials was necessary in all cases. The fact that the mean value of this renormalization factor ($< N >= 1.34$) is close to the unity constitutes a justification of the folding model. The value slightly higher than one can be related to the threshold anomaly recently put in evidence in the interaction of heavy-ions near the Coulomb barrier .

The oscillatory pattern observed at intermediate angles for some mass systems has been explained by the interference between the elastic transfer and the direct elastic scattering. In the case of one nucleon and α transfers a very good agreement with the data is obtained by DWBA calculations using the spectroscopic factors deduced from reactions induced by light-ions. In the other cases when no reference value was available in the literature the spectroscopic factors were deduced by fitting the experimental data. Reasonable values were obtained, which support the elastic transfer reaction as the origin of such oscillations. A definitive proof of the role of the elastic transfer would be the stability with the incident energy of the oscillation phase. This has been demonstrated in the case of the two neutron transfer ($^{32}S+^{34}S$) and of the α transfer ($^{32}S+^{28}Si$) , systems previously studied at various incident energies.

A further analysis of the oscillating angular distributions has been pursued by introducing a parity dependent term in the optical potential. No special sensitivity to the

shape of this term was found. In fact only the sign of the parity dependent potential and its magnitude in the vicinity of the strong absorption radius can be deduced without ambiguity from the experimental data. It was found that a parity potential of only a few percent of the folding potential is able to produce oscillations. The same quality of fits than in the DWBA analysis was obtained, in particular no angular shifts were observed. This means that a simple parity dependent term added to the standard optical potential can simulate very well the elastic transfer or more complex antisymmetrization effects.

These results have been compared to the microscopic calculations of D. Baye in the two-centre harmonic oscillator shell-model. A total agreement between the predicted signs and the fitted ones has been obtained in the seven cases where oscillations are present. A comparison between the calculated parity radius (R_p) and the experimental strong-absorption radius (R_{SA}) shows that parity effects are present even if R_p is two or three fermis smaller than R_{SA} although we have shown that only the value of the parity dependent potential in a zone of about two fermis centered in R_{SA} may have an influence on the cross section. Thus we think that the antisymmetrization effects are underestimated by the model of D. Baye as it is applied in ref. [24]). This is probably due to the use of the harmonic oscillator functions. It would be interesting to use shell model functions with a correct asymptotic behaviour. It is possible in that model (see ref. [24])) but requires more extensive calculations. We also pointed out the possible role of cluster effects or sequential transfer mechanisms which are not taken into account in the model.

Acknowledgments

The authors wish to express their gratitude to D.Baye for his constant interest and for stimulating discussions and to L.Stuttgé for her help during the experiments and the carefull reading of the manuscript. One of us (J.A.R.) is grateful to the Ministerio de Educacion y Ciencia for a fellowship and to the CRN (Strasbourg) for its hospitality.

Table 1.
Folding optical potentials

SYSTEM	E_{lab} (MeV)	N	$-W$ (MeV)	R_W (fm)	a_W (fm)	σ_R (mb)	$l_g^{a)}$	$R_{SA}^{b)}$ (fm)	$-NV_F(R_{SA})$ (MeV)	$-W(R_{SA})$ (MeV)
$^{37}Cl+^{40}Ca$	120.5	1.11	50.0	8.41	0.506	1045	42.2	10.76	0.967	0.476
$^{32}S+^{36}S$	90.0	1.69	50.0	8.05	0.503	944	32.8	10.47	0.713	0.404
	97.0	1.57	50.0	7.94	0.509	1080	36.5	10.35	0.826	0.435
$^{32}S+^{34}S$	97.1	1.31	50.0	7.95	0.477	967	33.7	10.25	0.913	0.399
$^{32}S+^{30}Si$	90.0	1.12	50.0	7.49	0.555	924	29.4	10.15	0.717	0.411
$^{32}S+^{28}Si$	90.0	1.20	50.0	7.65	0.471	752	25.7	9.88	0.974	0.435
$^{31}P+^{32}S$	86.5	1.37	50.0	8.15	0.391	734	26.9	10.12	0.905	0.322
$^{31}P+^{29}Si$	85.9	1.50	50.0	7.49	0.485	854	27.4	9.92	0.882	0.331
$^{31}P+^{28}Si$	85.9	1.33	50.0	7.56	0.488	839	26.6	9.98	0.790	0.349
$^{31}P+^{27}Al$	79.5	1.19	50.0	7.37	0.483	732	23.4	9.85	0.839	0.293

a) l_g is defined by $1-|S_{l_g}|=1/2$
b) $R_{SA}=\frac{1}{k}\{n+(n^2+l_g(l_g+1))^{1/2}\}$

Table 2.
Bound states characteristics

SYSTEM $x+A$	I_x	N	L	J	$-V^{a)}$ (MeV)	$r_0^{b)}$ (fm)	a_0 (fm)	ε (MeV)	$\tilde{S}^{c)}$	$\tilde{S}^{d)}_{exp}$	$\tilde{S}_{th}$
p+^{31}P	1/2	1	0	1/2	57.9	1.25	0.65	−8.86	1.0	1.0 ± 0.1	1.29[i)]
2n+^{32}S	0	2	0	0	74.6	1.25	0.65	−20.06	1.7		
2p+^{30}Si	0	2	0	0	88.9	1.25	0.65	−16.16	2.0		2.33[j)]
d+^{29}Si	1	2	0	1	80.6	1.25	0.65	−15.68	1.1		
3p+^{37}Cl	1/2	1	1	3/2	78.7	1.25	0.65[f)]	−24.95			
t+^{28}Si	1/2	3	0	1/2	99.4	1.25	0.65	−17.90	0.6	0.14[g)]	
4n+^{32}S	0	4	0	0	105.	0.97[e)]	0.65	−36.94	≤ 0.24		
α+^{28}Si	0	4	0	0	82.3	0.97[e)]	0.65	−6.94	0.24	0.22[h)]	0.09[k)]
α+^{27}Al	0	3	2	2	86.2	0.97[e)]	0.65	−9.67	≤ 0.24		0.09[k)]

[a)] Woods-Saxon potential with r_0 and a_0 fixed and V fitted to generate a (N, L, J) state with energy ε.
[b)] $R_V = r_0 A^{1/3}$
[c)] Spectroscopic factors used in the present analysis ($\tilde{S} = C^2S$).
[d)] Deduced from light-ion reactions[34]).
[e)] $R_V = r_0(A^{1/3} + 4^{1/3})$
[f)] A spin-orbit potential $V_{SO} = 6$ MeV was introduced.
[g)] Ref. [36]) [h)] Ref. [37]) [i)] Ref. [35]) [j)] Ref. [40]) [k)] Ref. [47])

Table 3.
Characteristics of the parity dependence

SYSTEM	R_{SA} (fm)	$V_p(R_{SA})^{a)}$ (MeV)	$V_{rp}^{b)}$	$C^{c)}$	$R_p^{d)}$ (fm)	sign$(V_p)^{d)}$
^{31}P+^{32}S	10.12	0.151	0.16	−0.18	11.8	+
^{31}P+^{29}Si	9.92	0.053	0.064	−0.06	9.4	+
^{32}S+^{30}Si	10.15	−0.087	0.12	0.12	9.3	−
^{32}S+^{34}S	10.25	−0.086	0.095	0.08	7.7	−
^{31}P+^{28}Si	9.98	−0.023	0.03	0.03	8.1	−
^{32}S+^{28}Si	9.88	−0.058	0.06	0.05	7.1	-
^{32}S+^{36}S	10.47	−0.008	< 0.01	< 0.01	3.2	−

[a)] $V_p(r)$ given by eq.(6)
[b)] $V_{rp} = \mid V_p(R_{SA})/NV_F(R_{SA}) \mid$
[c)] Deduced by fitting experimental data with $V_p(r) = CNV_F(r)$
[d)] From [24])

References

(1) W. von Oertzen and H. G. Bohlen, Phys. Reports **19C** (1975) 1

(2) D. F. Hebbard, J. Nurzynski, T. R. Ophel, P. V. Drumm, Y. Kondō, B. A. Robson and R. Smith, Nucl. Phys. **A461** (1988) 161

(3) S. Kubono, P. D. Bond, D. Horn, C. E. Thorn, Phys. Lett. **84B** (1979) 408
S. Kubono, P. D. Bond and C. E. Thorn, Phys. Lett. **81B** (1979) 140
S. Kubono, P. D. Bond, D. Horn and T. R. Renner, Phys. Rev. **C21** (1980) 459

(4) Y. D. Chan, R. J. Puigh, W. L. Lynch, M. Y. Tsang and J. G. Cramer, Phys. Rev. **C25** (1982) 850

(5) Chenqun Gao, Pingzhi Ning and Guozhu He, Nucl. Phys. **A438** (1985) 281

(6) N. Cindro, D. Počanić, D. M. Drake, J. D. Moses, J. C. Peng, N. Stein and J. W. Sunier, Nucl. Phys. **A459** (1986) 438

(7) B. Bilwes, R. Bilwes, J. Díaz, J. L. Ferrero, D. Počanić and L. Stuttgé, Nucl. Phys. **A463** (1987) 731

(8) C. K. Gelbke, R. Bock and A. Richter, Phys. Rev. **C9** (1974) 852

(9) B. Bilwes, R. Bilwes, V. D'Amico, J. Díaz, J. L. Ferrero, A. Italiano, R. Potenza, C. Roldan, A. Strazzeri and C. Tuvé, Nucl. Phys. **A468** (1987) 177

(10) M. C. Mermaz, B. Bilwes, R. Bilwes and J. L. Ferrero, Phys. Rev. **C27** (1983) 2408

(11) W. E. Frahn, in Treatise of Heavy-Ion Science, ed D. A. Bromley, vol.1, (Plenum Press, N.Y., 1984) p.264

(12) O. Tanimura, Lecture Notes in Physics **156** (1982) 372
B. A. Robson and R. Smith, Phys. Lett. **123B** (1983) 160
Y. Kondō, B. A. Robson and R. Smith, Nucl. Phys. **A410** (1983) 289

(13) Y. Kondō, B. A. Robson, R. Smith and H. H. Wolter Phys. Lett. **162B** (1985) 39
W. J. Naudé, H. S. Bradlow, O. Dietzsch, A. A. Pilt, W. D. M. Rac and D. Sinclair, Z. Phys. **A311** (1983) 297
W. N. Reisdorf, P. H. Lau and R. Vandenbosch, Nucl. Phys. **A253** (1975) 490
A. Barbadoro, D. Consolaro, F. Pellegrini, L. Taffara, D. Trivisonno, M. Bruno, I. Grabrielli, Nuovo Cimento **A95** (1986) 197

(14) J. Sromicki, M. Hugi, J. Lang, R. Müller, E. Ungricht, L. Jarczyk, B. Kamys, A. Mageira, Z. Rudy, A. Strzalkowski and B. Zebik, Nucl. Phys. **A406** (1983) 390

(15) A. Kabir, M. W. Kermode and N. Rowley, Nucl. Phys. **A481** (1988) 94

(16) A. M. Kobos and G. R. Satchler, Nucl. Phys. **A427** (1984) 589

(17) in collaboration with J. Chaumont, R. Meunier, Laboratoire Bernas, Orsay

(18) Target Labor, GSI- Darmstadt (Germany)

(19) A. Saettel, CRN-Strasbourg

(20) A. Baeza, B. Bilwes, R. Bilwes, J. Díaz and J. L. Ferrero, Nucl. Phys. **A419** (1984) 412

(21) B. Bilwes, R. Bilwes, V. D'Amico, J. L. Ferrero, R. Potenza and G. Giardina, Nucl. Phys. **A408** (1983) 173

(22) Rapport d'activité CRN-Strasbourg (1986) p. 131

(23) Y. C. Tang, Lecture notes in Physics, vol. 145 (Springer-Verlag, Berlin,1980) p. 572

(24) D. Baye, Nucl. Phys. **A460** (1986) 581

(25) S. Kubono, D. A. Lewis and D. Dehnhard, Nucl. Phys. **A334** (1980) 336

(26) G. Bertsch, J. Borysowicz, H. McManus and W. G. Love, Nucl. Phys. **A284** (1977) 399

(27) H. de Vries, C. W. de Jager and C. de Vries, Atomic Data and Nuclear Data Tables **36** (1987) 495

(28) G. D. Alkhazov, S. L. Belostotsky, O. A. Domchenkov, Yu. V. Dotsenko, N. P. Kuropatkin, M. A. Schuvaev and A. Vorobyov, Phys. Lett. **57B** (1975) 47

(29) Computer code ECIS, J. Raynal, Phys. Rev. **C23** (1981) 2571
(30) A. J. Baltz, P. D. Bond, J. D. Garrett and S. Kahana, Phys. Rev. **C12** (1975) 136
(31) G. R. Satchler and W. G. Love, Phys. Reports **55** (1979) 183
G. R. Satchler, Nucl. Phys. **A329** (1979) 233
(32) C. Mahaux, H. Ngô and G. R. Satchler, Nucl. Phys. **A449** (1986) 354
(33) Computer code PTOLEMY, M. H. Macfarlane and S. C. Pieper, ANL Report ANL-76-11 Rev. 1, 1978
(34) P. M. Endt, Atomic and Nuclear Data Tables **19** (1977) 23
(35) B. H. Wildenthal, J. B. McGrory, E. C. Halbert and H. D. Graber, Phys. Rev. **C4** (1971) 1708
(36) K Jankowski, A. Grzeszczuk, M. Siemaszko, A. Surowiec, W. Zipper, A. Budzanowski and E. Kozik, Nucl. Phys. **A426** (1984) 1
(37) W. Oelert, G. P. A. Berg, A. Djaloeis, C. Mayer-Böǐick and P. Turek, Phys. Rev. **C38** (1983) 73
(38) G. R. Satchler, Direct Nuclear Reactions, (Oxford University Press, N. Y., 1983), p. 86
(39) J. Díaz, J. L. Ferrero, J. A. Ruiz, B. Bilwes and R. Bilwes, Nucl. Phys. **A494** (1989) 311
(40) F. Sanchez, Thesis 1989, University of Valencia (Spain)
J. Díaz, J. L. Ferrero, F. Sanchez, B. Bilwes and R. Bilwes , Lecture Notes in Physics **317** (1988) 40
(41) Guozhu He, Chengqun Gao and Pingzhi Ning, Phys. Rev. **C30** (1984) 534
(42) M. A. Franey, V. Shkolnik and D. Dehnhard, Phys. Lett. **81B** (1979) 132
(43) A. Vitturi and C. H. Dasso, Nucl. Phys. **A458** (1986) 157
(44) V. N. Bragin, G. Pollarolo and A. Winter, Nucl. Phys. **A456** (1986) 475
(45) M. S. Hussein, L. F. Canto and R. Donangelo, Phys. Rev. **C29** (1984) 2383
(46) B. Kohlmeyer, Thesis 1973, University of Marburg (Germany)
(47) W. Chung, J. van Hienen, B. H. Wildenthal and C. L. Bennett, Phys. Lett. **79** (1978) 381

Figure captions

Fig. 1 : Angular distribution of $^{31}P + ^{32}S$ elastic scattering. The dashed curve is the optical model calculation with the parameters of table 1. The dash-dotted curve is the DWBA calculation of the elastic transfer with the same optical potential and the bound-state parameters and the spectroscopic factor of table 2. The solid line is obtained by adding coherently the two precedent amplitudes (see eq. 1).

Fig. 2 : The same as figure 1 but for the systems differing by two nucleons: $^{31}P+^{29}Si$ (1d), $^{32}S+^{30}Si$ (2p) and $^{32}S+^{34}S$ (2n).

Fig. 3 : The same as figure 1 but for the systems differing by three nucleons: $^{31}P+^{28}Si$ (1t) and $^{37}Cl+^{40}Ca$ (3p). In the latter case the dash-dotted curve is an estimation of the total cross section (sum of the components $l = 0, 1, 2$ with $\tilde{S} = 1$). The estimated yield of this reaction is so small that the effect on the elastic cross section must be negligeable.

Fig. 4 : The same as figure 1 but for the system differing by four neutrons: $^{32}S+^{36}S$ at two incident energies. The spectroscopic factor used is $\tilde{S} = 0.24$.

Fig. 5 : The same as figure 1 but for the systems differing by an α: $^{32}S+^{28}Si$ and $^{31}P+^{27}Al$. In this latter case the cross section of the interferring $l = 0$ component is very low and consequently the expected oscillations are negligible.

Fig. 6 : Coordinate definitions for the transfer of a cluster x between two cores b and A.

Fig. 7 : Parity dependent potential analysis of $^{31}P+^{32}S$ elastic scattering. The dashed curve is obtained without parity dependent term (identical to the dashed curve in figure 1). The solid curve is obtained with the parity dependent term (eq. 6) whose parameters are given in table 2.

Fig. 8 : The same as figure 7 but for the case of nuclei differing by two nucleons.

Fig. 9 : The same as figure 7 but for the case of $^{31}P+^{28}Si$.

Fig. 10 : The same as figure 7 but for the case of $^{32}S+^{36}S$ and $^{32}S+^{28}Si$.

Fig. 11 : Comparison of the parity dependent part of the optical potential obtained by fitting the $^{32}S+^{28}Si$ data with different parametrizations. Here $V_F(r)$ is the folding potential renormalized by the factor N given in table 1 (see section 3). The curve labelled with D is the parity potential $V_\pi(r)$ of the form given by eq. (6) and the signs between brackets indicate the sign of that potential.

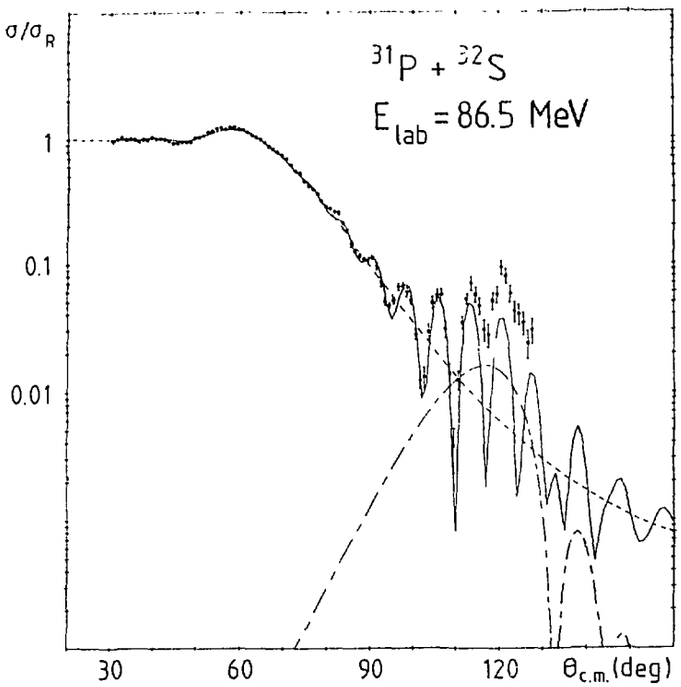
σ/σR
31P + 32S
Elab = 86.5 MeV
1
0.1
0.01
30
60
90
120
θc.m.(deg)

Fig. 1

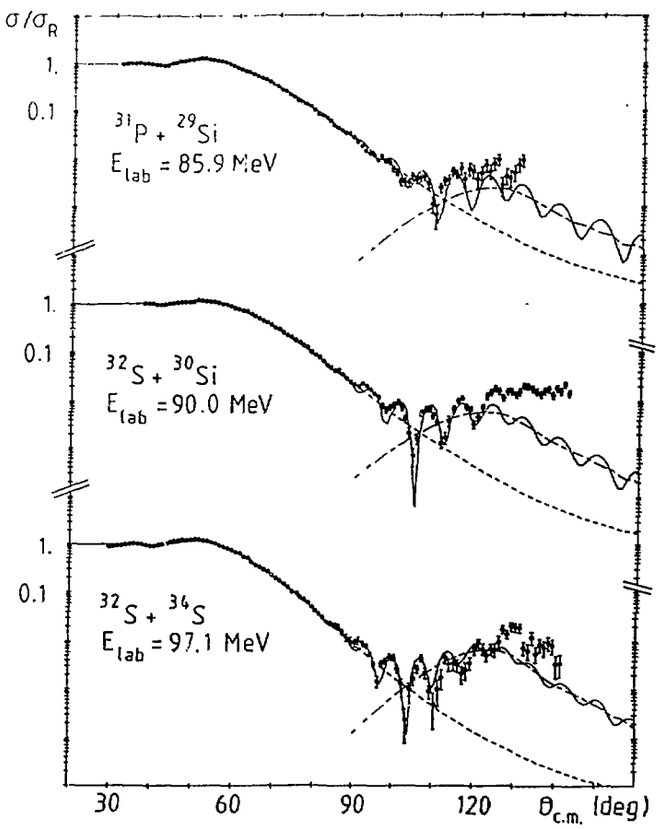
σ/σR
1.
0.1
31P + 29Si
Elab = 85.9 MeV
32S + 30Si
Elab = 90.0 MeV
32S + 34S
Elab = 97.1 MeV
30
60
90
120
θc.m. (deg)

Fig. 2

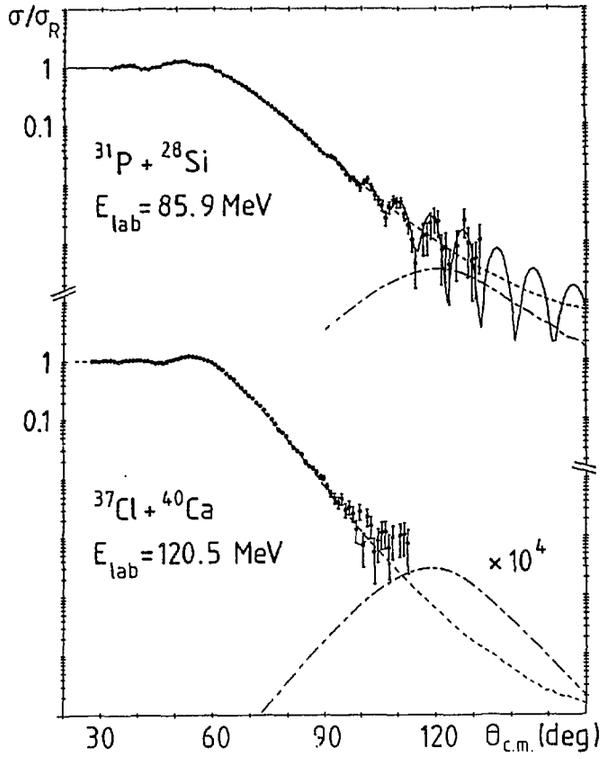
σ/σR
1
0.1
31P + 28Si
Elab = 85.9 MeV
1
0.1
37Cl + 40Ca
Elab = 120.5 MeV
× 10^4
30
60
90
120
θc.m. (deg)

Fig. 3

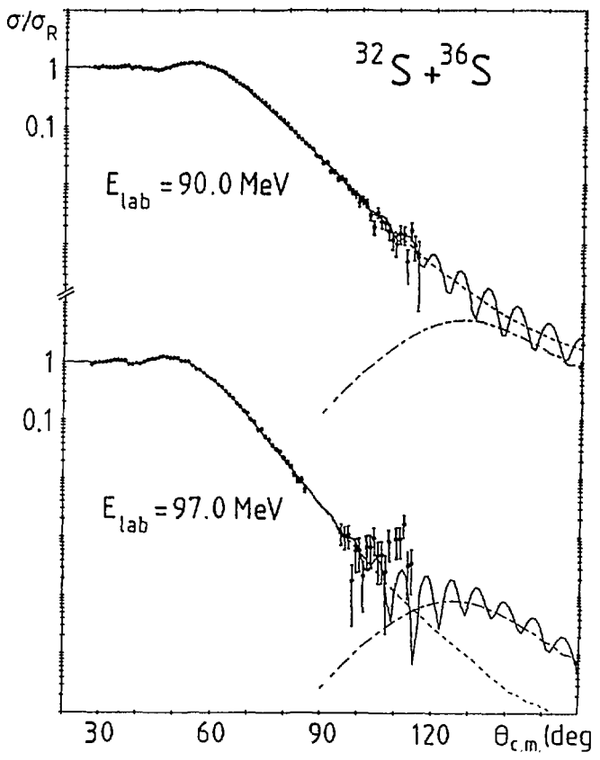
σ/σR
32S + 36S
1
0.1
Elab = 90.0 MeV
1
0.1
Elab = 97.0 MeV
30
60
90
120
θc.m. (deg

Fig. 4

g)

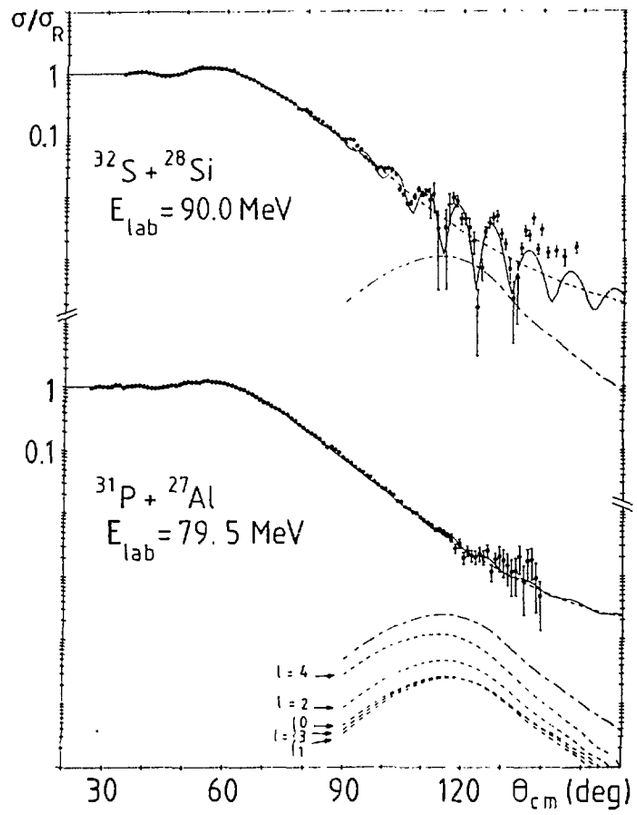
σ/σR
1
0.1
32S + 28Si
Elab = 90.0 MeV
1
0.1
31P + 27Al
Elab = 79.5 MeV
l = 4
l = 2
l = 0
l = 3
l = 1
30
60
90
120
θcm (deg)

Fig. 5

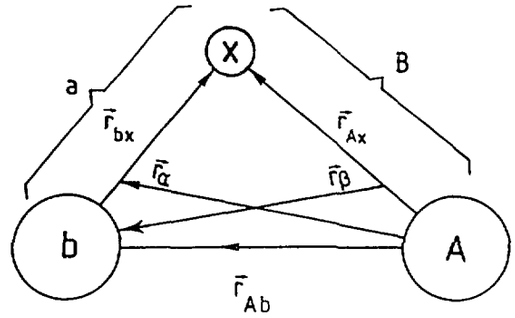
X
a
B
r̄bx
r̄Ax
r̄α
r̄β
b
A
r̄Ab

Fig. 6

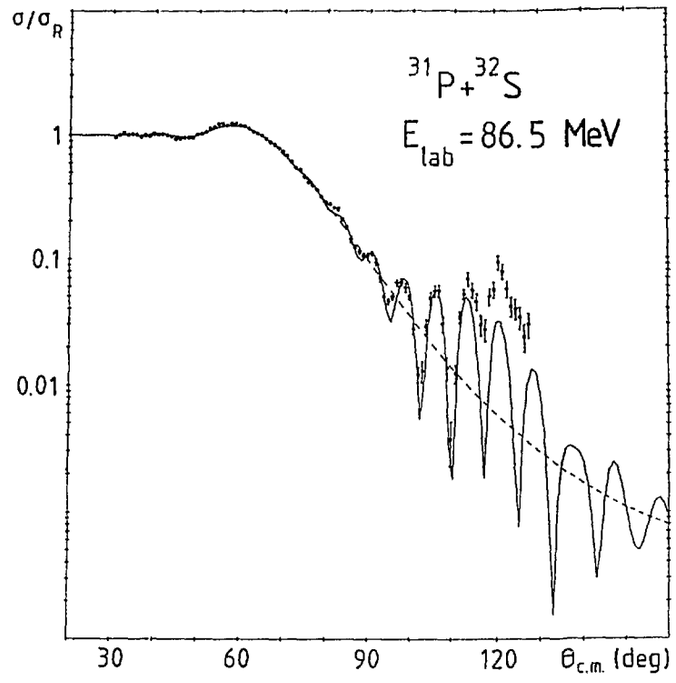
σ/σR
1
0.1
0.01
31P+32S
Elab=86.5 MeV
30
60
90
120
θc.m. (deg)

Fig. 7

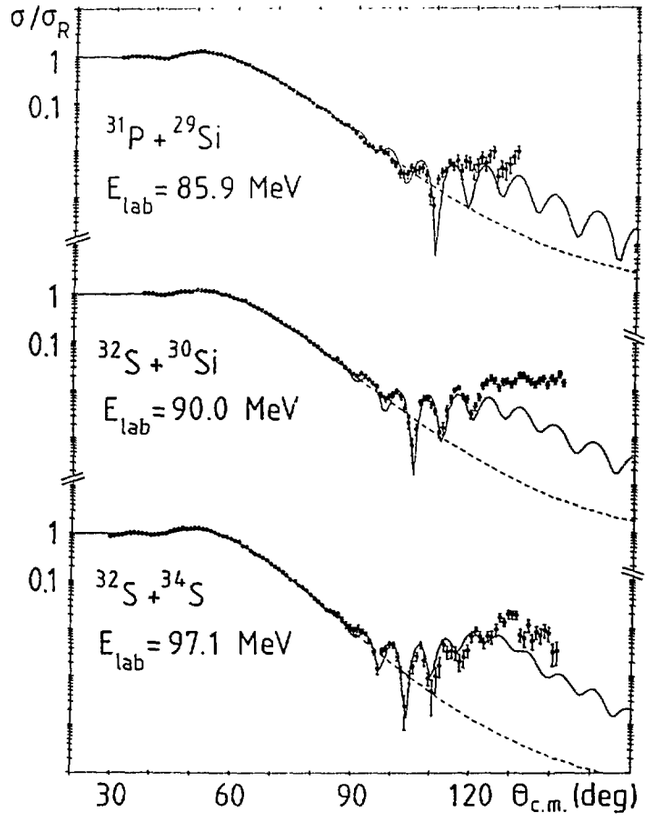
σ/σR
1
0.1
31P + 29Si
Elab= 85.9 MeV
1
0.1
32S + 30Si
Elab= 90.0 MeV
1
0.1
32S + 34S
Elab= 97.1 MeV
30
60
90
120
θc.m. (deg)

Fig. 8

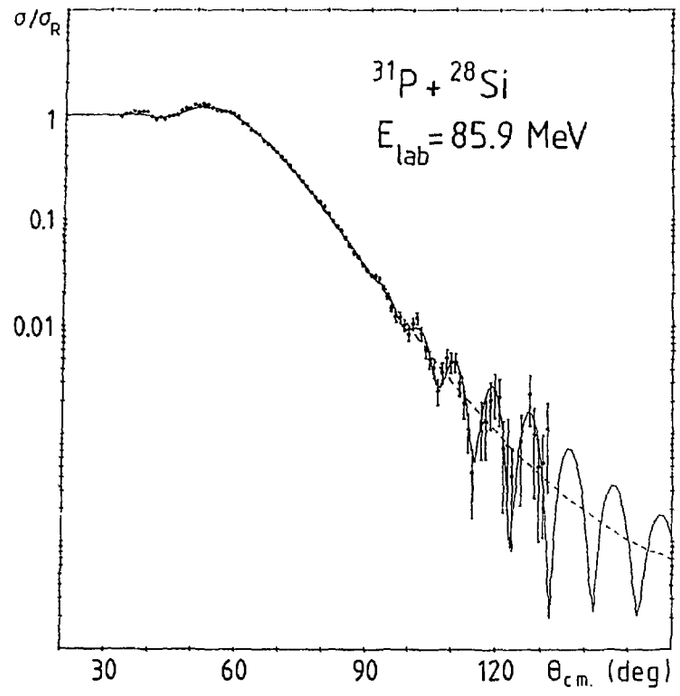
σ/σR
1
0.1
0.01
31P + 28Si
Elab = 85.9 MeV
30
60
90
120
θc.m. (deg)

Fig. 9

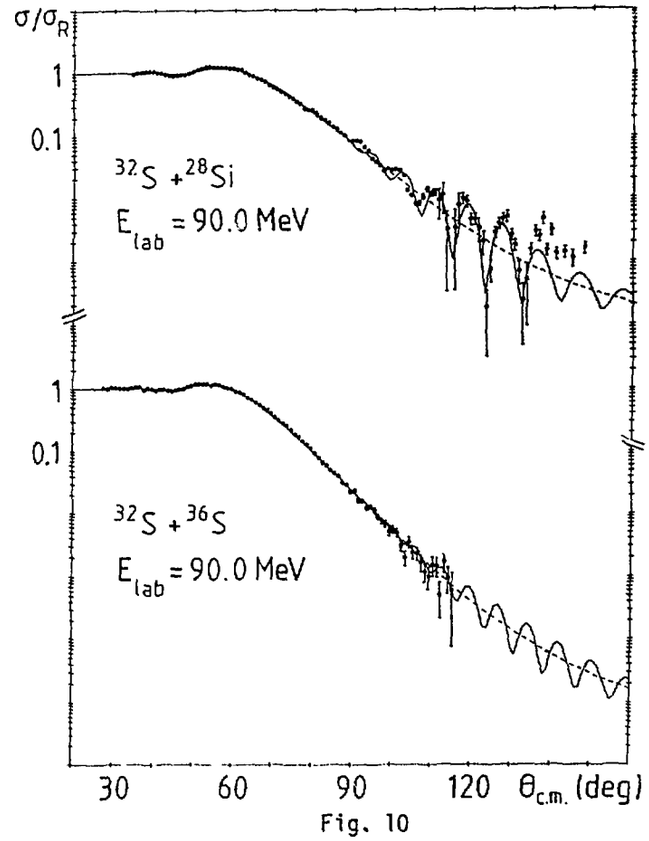
σ/σR
1
0.1
32S + 28Si
Elab = 90.0 MeV
1
0.1
32S + 36S
Elab = 90.0 MeV
30
60
90
120
θc.m. (deg)

Fig. 10

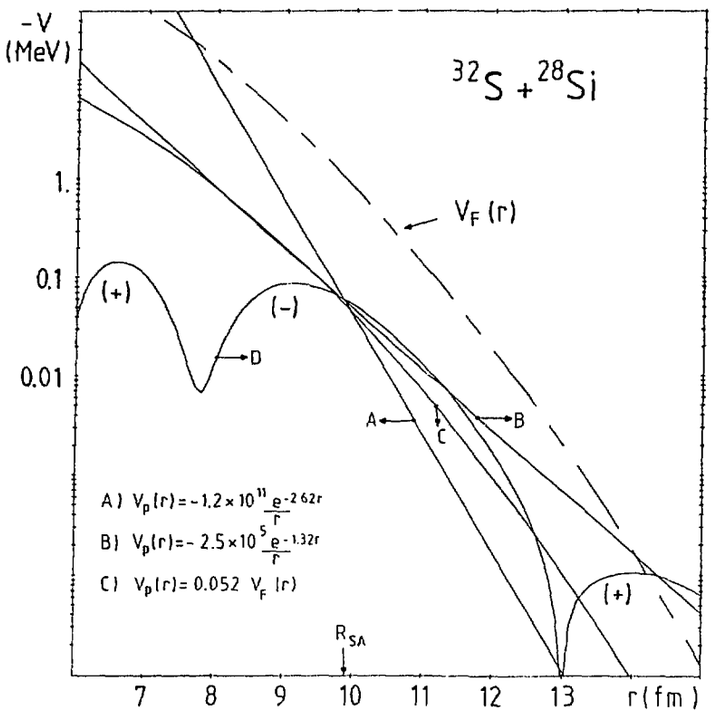
-V
(MeV)
$^{32}S + ^{28}Si$
1.
0.1
0.01
V_F (r)
(+)
(-)
D
A
C
B
A) $V_p(r) = -1.2 \times 10^{11} \frac{e^{-2.62r}}{r}$
B) $V_p(r) = -2.5 \times 10^{5} \frac{e^{-1.32r}}{r}$
C) $V_p(r) = 0.052\ V_F(r)$
(+)
R_{SA}
7
8
9
10
11
12
13
r(fm)

Fig. 11

eg)

Imprimé
au Centre de
Recherches Nucléaires
Strasbourg
1989